



## Article

# Exploring the Diversity and Dehydration Performance of New Mixed Tutton Salts ( $K_2V_{1-x}M'_x(SO_4)_2(H_2O)_6$ , Where $M' = Co, Ni, Cu, \text{ and } Zn$ ) as Thermochemical Heat Storage Materials

João G. de Oliveira Neto<sup>1,\*</sup>, Jacivan V. Marques<sup>1</sup>, Jayson C. dos Santos<sup>1</sup>, Adenilson O. dos Santos<sup>1</sup>   
and Rossano Lang<sup>2,\*</sup> 

<sup>1</sup> Center for Social Sciences, Health and Technology, Federal University of Maranhão—UFMA, Imperatriz 65900-410, MA, Brazil; jacivan.vm@discente.ufma.br (J.V.M.); jayson.cabral@discente.ufma.br (J.C.d.S.); adenilson.santos@ufma.br (A.O.d.S.)

<sup>2</sup> Institute of Science and Technology, Federal University of São Paulo—UNIFESP, São José dos Campos 12231-280, SP, Brazil

\* Correspondence: joao.gon@ufma.br (J.G.d.O.N.); rossano.lang@unifesp.br (R.L.)

**Abstract:** Tutton salts form an isomorphic crystallographic family that has been intensively investigated in recent decades due to their attractive thermal and optical properties. In this work, we report four mixed Tutton crystals (obtained by the slow solvent evaporation method) with novel chemical compositions based on  $K_2V_{1-x}M'_x(SO_4)_2(H_2O)_6$ , where  $M'$  represents Co, Ni, Cu, and Zn, aiming at thermochemical energy storage applications. Their structural and thermal properties were correlated with theoretical studies. The crystal structures were solved by powder X-ray diffraction using the Rietveld method with similar compounds. All of the samples crystallized in monoclinic symmetry with the  $P2_1/a$ -space group. A detailed study of the intermolecular interactions based on Hirshfeld surfaces and 2D fingerprint mappings showed that the main interactions arise from hydrogen bonds ( $H\cdots O/O\cdots H$ ) and dipole–ion ( $K\cdots O/O\cdots K$ ). On the other hand, free space percentages in the unit cells determined by electron density isosurfaces presented low values ranging from 0.53 (V–Ni) to 0.81% (V–Cu). The thermochemical findings from thermogravimetry, a differential thermal analysis, and differential scanning calorimetry indicate that  $K_2V_{0.47}Ni_{0.53}(SO_4)_2(H_2O)_6$  salt is the most promising among mixed salts ( $K_2V_{1-x}M'_x(SO_4)_2(H_2O)_6$ ) for heat storage potential, achieving a low dehydration temperature ( $\approx 85^\circ C$ ), high dehydration enthalpy ( $\approx 360$  kJ/mol), and high energy storage density ( $\approx 1.84$  GJ/m<sup>3</sup>).

**Keywords:** crystal growth; mixed Tutton salts; powder X-ray diffraction; Hirshfeld surfaces; crystal voids; thermal analysis; thermochemical heat storage



**Citation:** Oliveira Neto, J.G.d.; Marques, J.V.; Santos, J.C.d.; Santos, A.O.d.; Lang, R. Exploring the Diversity and Dehydration Performance of New Mixed Tutton Salts ( $K_2V_{1-x}M'_x(SO_4)_2(H_2O)_6$ , Where  $M' = Co, Ni, Cu, \text{ and } Zn$ ) as Thermochemical Heat Storage Materials. *Physchem* **2024**, *4*, 319–333. <https://doi.org/10.3390/physchem4030022>

Academic Editor: Rocco Caliandro

Received: 30 July 2024

Revised: 18 August 2024

Accepted: 22 August 2024

Published: 26 August 2024



**Copyright:** © 2024 by the authors. Licensee MDPI, Basel, Switzerland. This article is an open access article distributed under the terms and conditions of the Creative Commons Attribution (CC BY) license (<https://creativecommons.org/licenses/by/4.0/>).

## 1. Introduction

Currently, society exists in the age of technology, fueled by an increasing demand for technological devices. This evolution has transformed our interactions with the world, affecting everything from communication to energy production and utilization [1]. Within this context, research in materials science has made significant advancements across various applications, leading to the development of new compounds that are efficient, sustainable, and adaptable to global requirements [2–4].

In a world constantly seeking sustainable energy solutions through technological advancements, vanadium compounds have emerged as promising candidates for a more efficient energy transition [5]. These compounds excel at storing energy in the form of flow batteries. Moreover, this metal possesses unique properties that make it suitable for diverse applications, including medicine, catalysts, and anti-corrosion coatings [6–8]. Its wide range of properties and various oxidation states contribute to its uniqueness in meeting technological demands [9]. Multiple synthesis routes allow for vanadium to be obtained in

different oxidation states. This study will explore its composition in the sulfated form and the oxidation state 2+ ( $V^{2+}$ ) [10,11].

Metal sulfate hydrates have been extensively investigated due to their potential for long-term thermochemical energy storage. These compounds offer advantages such as easy availability, low cost, and diverse applications across various research fields [12]. A study by Donkers et al. explored 563 salt hydrate reactions to assess their theoretical possibilities and limitations as thermochemical materials for energy storage in domestic environments [13]. The research established thermodynamic criteria for acceptable system performance. To evaluate a broader range of hydrates, Kooijman et al. considered specific criteria: an energy storage density of  $\geq 1.3 \text{ GJ/m}^3$ , a dehydration temperature of  $\leq 120 \text{ }^\circ\text{C}$ , water vapor pressure during dehydration of  $\leq 12 \text{ mbar}$ , and a minimum of 10 rehydration cycles [14]. Based on these criteria, the Tutton salts class has emerged as a promising candidate for thermochemical heat storage.

Tutton salts constitute a significant group of inorganic crystals characterized by their isomorphic hexahydrate structure, described by the general chemical formula  $M^I_2M^{II}(XO_4)_2(H_2O)_6$ , where  $M^I$  represents a monovalent cation (such as  $K^+$ ,  $NH_4^+$ ,  $Rb^+$ , or  $Cs^+$ ),  $M^{II}$  denotes a bivalent cation ( $Mg^{2+}$ ,  $Co^{2+}$ ,  $Ni^{2+}$ ,  $V^{2+}$ ,  $Fe^{2+}$ , or  $Zn^{2+}$ ), and  $X$  represents a site containing elements with a high oxidation state, such as S or Se [15,16]. These hydrate double salts crystallize in a monoclinic system with the  $P2_1/a$ -space group [17]. They exhibit dielectric properties and, in specific cases, demonstrate antiferromagnetic ordering at low temperatures [18]. Each unit cell contains two formulas ( $Z = 2$ ). The crystal structure involves intermolecular interactions between  $[M'(H_2O)_6]^{2+}$  octahedral units and  $[XO_4]^{2-}$  tetrahedral layers, with the metal complex being situated at a center of inversion and slightly distorted due to the Jahn–Teller effect [19,20].

The physicochemical properties of Tutton salts can be fine-tuned by incorporating dopants or introducing two similar chemical species into the same structural site [21,22]. When two ions concomitantly occupy these sites, they form a subclass known as mixed Tutton salts [23]. These materials often exhibit enhanced thermochemical and optical characteristics compared to individual Tutton salts. For instance, crystals like  $K_2Mn_{0.03}Ni_{0.97}(SO_4)_2(H_2O)_6$ ,  $K_2Mn_{0.18}Cu_{0.82}(SO_4)_2(H_2O)_6$  [24],  $K_2Zn_{0.60}Mg_{0.40}(SO_4)_2 \cdot 6H_2O$  [25], and  $(NH_4)_2Mn_{(1-x)}Zn_{(x)}(SO_4)_2(H_2O)_6$  [17] have demonstrated improved properties. Despite their potential, no study has reported the synthesis, structure solving, and properties of mixed Tutton salts containing vanadium as far as we know.

The present study aims to shed light on novel mixed Tutton salts with the composition  $K_2V_{1-x}M'_x(SO_4)_2(H_2O)_6$ , where  $M' = Co, Ni, Cu, \text{ and } Zn$ , and to evaluate their potential as thermochemical materials. The structures of the mixed Tutton salts were solved by powder X-ray diffraction (PXRD) using the Rietveld refinement method. The influence of the  $V^{2+}$  and  $M'$  species was detailed from a computational study of intermolecular interactions and unit cell voids by using Hirshfeld surfaces and crystal voids (electron density isosurfaces), respectively. Thermogravimetry (TG), differential thermal analysis (DTA), and differential scanning calorimetry (DSC) were used to estimate the thermochemical parameters. The results show that the  $K_2V_{0.47}Ni_{0.53}(SO_4)_2(H_2O)_6$  salt is the most promising among the mixed  $K_2V_{1-x}M'_x(SO_4)_2(H_2O)_6$  salts for heat storage potential, achieving a low dehydration temperature ( $\approx 85 \text{ }^\circ\text{C}$ ), high dehydration enthalpy ( $\approx 360 \text{ kJ/mol}$ ), and high energy storage density ( $\approx 1.84 \text{ GJ/m}^3$ ).

## 2. Materials and Methods

### 2.1. Crystals Growth

Crystals with the composition  $K_2V_{1-x}M'_x(SO_4)_2(H_2O)_6$  (where  $M' = Co, Ni, Cu, \text{ and } Zn$ ) were synthesized from aqueous solutions by the isothermal evaporation method. The precursor compounds (>99%, Sigma Aldrich, Darmstadt, Germany) and their respective amounts are listed in Table 1. All reagents were solubilized in 50 mL of deionized water at  $50 \text{ }^\circ\text{C}$  under constant magnetic stirring (360 RPM) for 480 min. Subsequently, the solutions

were filtered, covered with a plastic film containing around 25 randomly distributed holes, and stored in a drying oven at 35 °C.

**Table 1.** Details regarding the proportions and quantities of precursor reagents used in crystal synthesis.

K <sub>2</sub> SO <sub>4</sub>		VOSO <sub>4</sub> ·x(H <sub>2</sub> O)		M'SO <sub>4</sub> (H <sub>2</sub> O) <sub>n</sub>		Sample Code	
[g]	[mol/L]	[g]	[mol/L]	[g]	[mol/L]		
1.045	0.10	0.2505	0.05	CoSO <sub>4</sub> (H <sub>2</sub> O) <sub>7</sub>	0.4216	0.05	KVCoSOH
1.045	0.10	0.2505	0.05	NiSO <sub>4</sub> (H <sub>2</sub> O) <sub>7</sub>	0.4113	0.05	KVNiSOH
1.045	0.10	0.2505	0.05	CuSO <sub>4</sub> (H <sub>2</sub> O) <sub>5</sub>	0.3745	0.05	KVCuSOH
1.045	0.10	0.2505	0.05	ZnSO <sub>4</sub> (H <sub>2</sub> O) <sub>7</sub>	0.4313	0.05	KVZnSOH

## 2.2. Structural Determination

The crystal structures were analyzed under room conditions using a PANalytical powder diffractometer (Empyrean model, Malvern Panalytical, Malvern, UK) with CuK $\alpha$  radiation ( $\lambda = 1.5418 \text{ \AA}$ ) operating at 40 kV/40 mA. The diffractograms were collected in the  $2\theta$  angular range between 10 and 50°, with a step of 0.02° and an acquisition time of 2 s. Subsequently, the PXRD patterns were indexed using mathematical algorithms implemented in DASH 4.0 software [26]. The Le Bail method was then applied to PXRD patterns to extract reflection intensities, determine atomic coordinates, and define cell parameters [27]. Starting structural parameters were accessed from the crystallographic information file (.cif), 50582 code of the Inorganic Crystal Structure Database (ICSD). Additionally, the Rietveld refinement method was used to refine the PXRD data until parameter optimization was achieved [28]. The final .cif files were validated with the enCIFer 2021.3 software [29] and deposited in the Cambridge Crystallographic Data Center (CCDC - Union Road, Cambridge CB2 1EZ, UK) under the following codes: 2363950 (KVCoSOH), 2363949 (KVNiSOH), 2363947 (KVCuSOH), and 2363946 (KVZnSOH). Copies of the structural data can be found, free of charge, via <https://www.ccdc.cam.ac.uk/structures/> (accessed on 30 May 2024).

## 2.3. Computational Studies

The non-covalent bonds of the crystalline systems were evaluated qualitatively and quantitatively based on calculations of Hirshfeld surfaces and their analogs using the Crystal Explorer 17.5 software [30]. Three-dimensional mappings were generated as a function of the normalized distance ( $d_{\text{norm}}$ ) using a three-color scheme in which the contacts most distant, similar, and close to the van der Waals radius ( $r_{\text{vdW}}$ ) are represented by the blue, white, and red, respectively. The percentage of each intermolecular contact was quantified from 2D fingerprint mappings plotted in terms of the distance from a given point on the Hirshfeld surface to the nearest off-surface atom ( $d_e$ ) and the distance from a given point on the Hirshfeld surface to the nearest atom within the surface ( $d_i$ ) [31]. Unit cell voids were estimated using the crystal void method identified by procrystal electron density isosurfaces [32].

## 2.4. Thermoanalytical Studies

Coupled TG-DTA measurements were performed on a Shimadzu thermal analyzer (model DTG-60, Shimadzu, Tokyo, Japan) in a temperature range between 27 and 900 °C with a heating rate of 10 °C/min under an inert N<sub>2</sub> gas atmosphere (100 mL/min). Fine powders of pulverized crystals were distributed into open alumina crucibles. The dehydration enthalpy was evaluated using DSC thermograms recorded by a DSC-60 thermal analyzer (Shimadzu, Tokyo, Japan). DSC analyses were conducted under the same experimental conditions as TG-DTA in a temperature range between 27 and 215 °C.

## 3. Results and Discussion

The KVCoSOH, KVNiSOH, KVCuSOH, and KVZnSOH salts were successfully crystallized using the isothermal evaporation method with deionized water as the solvent.

The samples grew under acidic conditions (pH  $\approx$  3.0–3.7) for approximately 14 to 21 days, resulting in dark blue single crystals with a prismatic morphology.

### 3.1. Structure Solving and Geometric Parameters

The four mixed salts exhibit similar PXRD patterns, as shown in Figure 1a. According to Rietveld refinement, all samples crystallize in monoclinic symmetry with the  $P2_1/a$ -space group containing two  $K_2V_{1-x}M'_x(SO_4)_2(H_2O)_6$  formulas per unit cell. The slight shifts observed in the peak positions correspond to the random occupation of the different divalent species (transition metals) on the structure and their respective occupancy factors. Table 2 summarizes all structural and cell parameters determined for the crystal series.

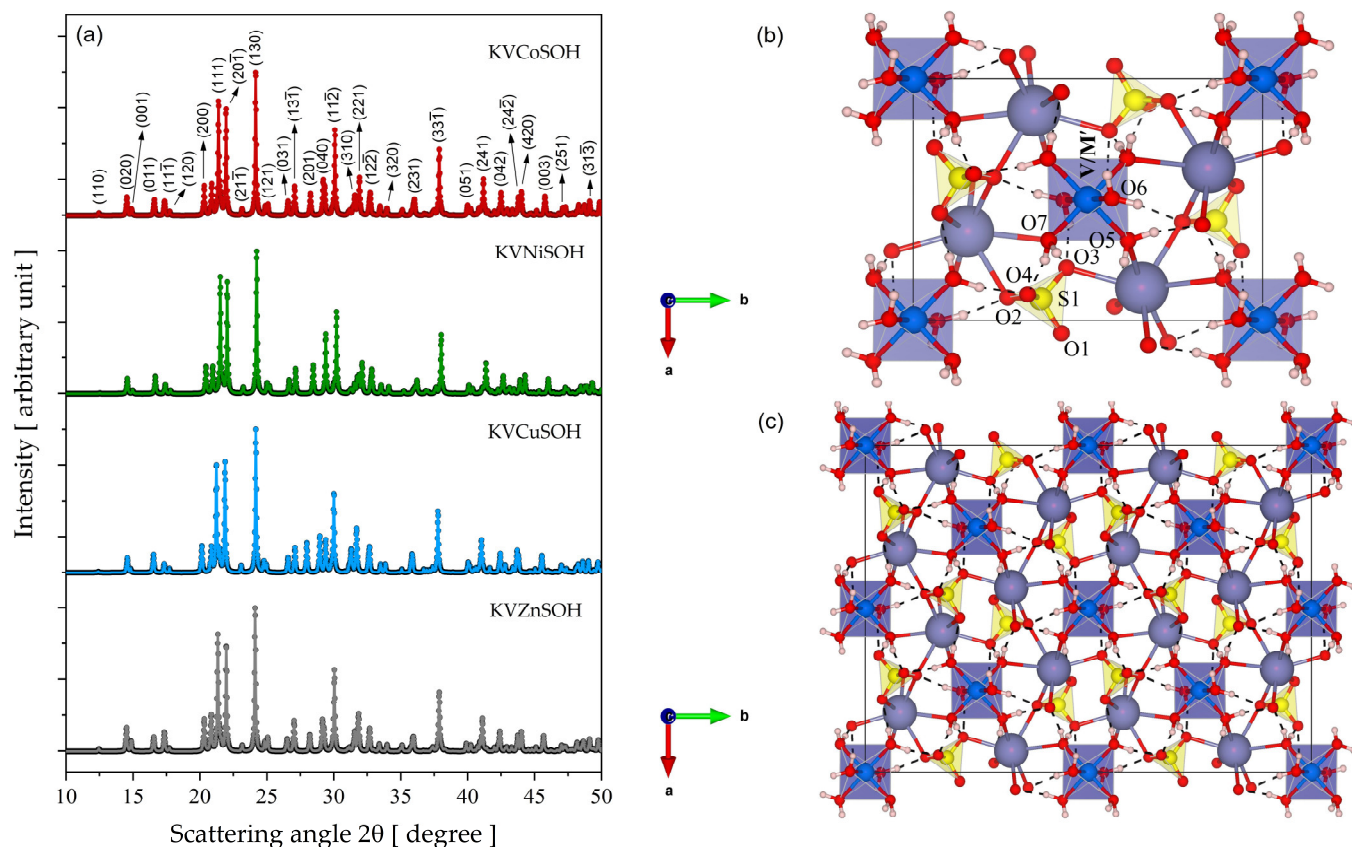


**Figure 1.** (a) PXRD patterns recorded under room conditions for KVCuSOH, KVNiSOH, KVCuSOH, and KVZnSOH samples; (b) Tutton salt unit cell in monoclinic system with labels along  $c$ -axis presenting intermolecular interactions; (c)  $2 \times 2 \times 2$  supercell to  $K_2V_{1-x}M'_x(SO_4)_2(H_2O)_6$  salts.

The crystallographic parameters in Table 2 confirm that all crystals belong to the isomorphic family of mixed Tutton salts. However, despite using an equimolar ratio between the  $VOSO_4 \cdot x(H_2O)$  and  $MSO_4(H_2O)_n$  compounds during synthesis, the nominal introduction of the divalent species into the crystal lattice was not guaranteed. Several physicochemical and experimental factors contribute to this, including the lack of control over the solvent evaporation rate, the formation of interfacial defects during crystallization, and electronegativity. It is also worth mentioning that the occupancy factors for each sample were estimated using the GSAS/EXPGUI software during the refinement procedure. Through several least squares cycles, the factors were reached. The mixed occupancy of the divalent species was further validated using the enCIFer 2021.3 software.

**Table 2.** Crystallographic parameters of KVM'SOH crystals obtained through refined PXRD patterns.

Sample	KVCoSOH	KVNiSOH	KVCuSOH	KVZnSOH
<b>Formula</b>	H <sub>12</sub> K <sub>2</sub> V <sub>0.48</sub> Co <sub>0.52</sub> O <sub>14</sub> S <sub>2</sub>	H <sub>12</sub> K <sub>2</sub> V <sub>0.47</sub> Ni <sub>0.53</sub> O <sub>14</sub> S <sub>2</sub>	H <sub>12</sub> K <sub>2</sub> V <sub>0.44</sub> Cu <sub>0.56</sub> O <sub>14</sub> S <sub>2</sub>	H <sub>12</sub> K <sub>2</sub> V <sub>0.49</sub> Zn <sub>0.51</sub> O <sub>14</sub> S <sub>2</sub>
<b>Formula weight [g/mol]</b>	433.51	433.46	436.41	436.73
<b>a [Å]</b>	9.033(4)	8.985(3)	9.094(2)	9.028(7)
<b>b [Å]</b>	12.171(8)	12.148(7)	12.144(7)	12.196(5)
<b>c [Å]</b>	6.144(7)	6.118(8)	6.164(9)	6.154(7)
<b>α [°]</b>	90.00	90.00	90.00	90.00
<b>β [°]</b>	104.78(7)	104.97(4)	104.41(6)	104.64(9)
<b>γ [°]</b>	90.00	90.00	90.00	90.00
<b>Volume [Å<sup>3</sup>]</b>	653.12(6)	645.26(4)	659.42(7)	655.59(7)
<b>Crystalline system</b>	Monoclinic	Monoclinic	Monoclinic	Monoclinic
<b>Space group</b>	<i>P</i> 2 <sub>1</sub> / <i>a</i>	<i>P</i> 2 <sub>1</sub> / <i>a</i>	<i>P</i> 2 <sub>1</sub> / <i>a</i>	<i>P</i> 2 <sub>1</sub> / <i>a</i>
<b>Rwp [%]</b>	8.33	9.32	9.59	9.89
<b>Rp [%]</b>	6.28	7.02	7.97	7.35
<b>S</b>	1.11	1.07	1.65	1.10

Additionally, the atomic radius plays a crucial role in accommodating divalent cations in a Tutton structure. For example, in the KVZnSOH sample, the V/Zn ratio was 0.49/0.51, probably due to a small difference (0.06 Å) between the atomic radii of V (2.07 Å) and Zn (2.01 Å). In contrast, for the KVNiSOH and KVniCuSOH samples, the difference between the V(2.07 Å)–Ni(1.97 Å) and V(2.07 Å)–Cu(1.96 Å) atomic radii reached 0.10 Å and 0.11 Å, respectively. The results suggest that crystals containing different divalent species with similar atomic radii tend to exhibit equivalent amounts of cations [24].

Figure 1b illustrates a projection of the primitive unit cell for the vanadium-based mixed Tutton salts, as the four materials are isostructural. The crystals are composed of three distinct layers: a slightly distorted [V/M'(H<sub>2</sub>O)<sub>6</sub>] hexahydrate complex, two [SO<sub>4</sub>] tetrahedra, and two irregular [KO<sub>8</sub>] polyhedra. These fragments propagate throughout the crystal lattice, forming a periodically ordered system based on intermolecular interactions, including hydrogen bonds and dipole–ion, as presented in Figure 1c.

To assess the Jahn–Teller effect on the [V/M'(H<sub>2</sub>O)<sub>6</sub>] octahedrons, we analyzed geometric parameters related to bond lengths and angles using the constituent atoms within the coordination sphere. The summarized data can be found in Tables 3 and 4.

**Table 3.** The bond lengths determined experimentally from the solved KVM'SOH structures.

KVCoSOH		KVNiSOH		KVCuSOH		KVZnSOH	
Bond	Length [Å]	Bond	Length [Å]	Bond	Length [Å]	Bond	Length [Å]
V/Co–O5	2.116(7)	V/Ni–O5	2.071(2)	V/Cu–O5	2.129(3)	V/Zn–O5	2.122(2)
V/Co–O6	2.127(8)	V/Ni–O6	2.079(8)	V/Cu–O6	2.133(4)	V/Zn–O6	2.129(3)
V/Co–O7	2.031(2)	V/Ni–O7	2.014(5)	V/Cu–O7	2.030(1)	V/Zn–O7	2.029(3)
S1–O1	1.472(5)	S1–O1	1.474(2)	S1–O1	1.470(2)	S1–O1	1.473(2)
S1–O2	1.456(3)	S1–O2	1.463(2)	S1–O2	1.469(2)	S1–O2	1.462(2)
S1–O3	1.471(9)	S1–O3	1.473(1)	S1–O3	1.485(2)	S1–O3	1.479(2)
S1–O4	1.47(8)	S1–O4	1.479(2)	S1–O4	1.481(3)	S1–O4	1.479(3)

From the data listed in Table 3, a uniaxial contraction can be seen around the V/M'–O5 axial bonds when compared to the V/M'–O6 and V/M'–O7 equatorial bonds, mainly for the KVZnSOH salt that presents the most significant difference (≈0.10 Å). The results then validate the Jahn–Teller effect, which corresponds to a spontaneous geometry distortion due to breaking in the *d*-orbitals degeneracy. Additionally, few differences are detected for the S–O bonds associated with [SO<sub>4</sub>] tetrahedrons, which indicates their almost perfect symmetry. Moreover, as shown in Table 4, the angles formed involving the axial bonds for all crystals are straight. In contrast, the other angles differ due to the “secondary” divalent

species ( $\text{Co}^{2+}$ ,  $\text{Ni}^{2+}$ ,  $\text{Cu}^{2+}$ , and  $\text{Zn}^{2+}$ ) and their respective occupancy factors since the  $\text{H}_2\text{O}$  ligands and the “primary” divalent species ( $\text{V}^{2+}$ ) are equivalent for all mixed Tutton salts.

**Table 4.** The bond angles determined experimentally from the solved KVM'SOH structures.

Sample M' = Co, Ni, Cu, and Zn	Bond Angle [°]			
	KVCoSOH	KVCoSOH	KVCoSOH	KVCoSOH
O5–V/M'–O5 *	180.0(0)	180.0(0)	180.0(0)	180.0(0)
O5–V/M'–O6 *	180.0(0)	180.0(0)	180.0(0)	180.0(0)
O5 *–V/M'–O6 *	180.0(0)	180.0(0)	180.0(0)	180.0(0)
O5–V/M'–O6	180.0(0)	180.0(0)	180.0(0)	180.0(0)
O5 *–V/M'–O6	91.0(3)	91.0(3)	91.0(3)	91.0(3)
O5 *–V/M'–O7 *	88.4(8)	88.4(8)	88.4(8)	88.4(8)
O5–V/M'–O7	89.3(3)	89.3(3)	89.3(3)	89.3(3)
O5–V/M'–O7 *	91.3(4)	91.3(4)	91.3(4)	91.3(4)
O5 *–V/M'–O7	88.9(7)	88.9(7)	88.9(7)	88.9(7)
O6–V/M'–O6 *	91.5(2)	91.5(2)	91.5(2)	91.5(2)
O6 *–V/M'–O7 *	90.6(7)	90.6(7)	90.6(7)	90.6(7)
O6–V/M'–O7 *	88.6(6)	88.6(6)	88.6(6)	88.6(6)
O6 *–V/M'–O7	88.9(7)	88.9(7)	88.9(7)	88.9(7)
O6–V/M'–O7	91.5(2)	91.5(2)	91.5(2)	91.5(2)
O1–S1–O2	90.6(7)	90.6(7)	90.6(7)	90.6(7)
O1–S1–O3	88.6(6)	88.6(6)	88.6(6)	88.6(6)
O1–S1–O4	91.0(3)	91.0(3)	91.0(3)	91.0(3)
O2–S1–O3	88.4(8)	88.4(8)	88.4(8)	88.4(8)
O2–S1–O4	89.3(3)	89.3(3)	89.3(3)	89.3(3)
O3–S1–O4	91.3(4)	91.3(4)	91.3(4)	91.3(4)

\*  $1 - x, -y, 1 - z$ .

### 3.2. Analysis of Intermolecular Interactions by Hirshfeld Surfaces

To better understand the structural and geometric parameters of vanadium-based Tutton salts, a qualitative computational study on non-covalent bonds using Hirshfeld surfaces was conducted. From the asymmetric units shown in Figure 2a–d and 3D mappings were generated based on  $d_{norm}$ , as depicted in Figure 2e–h. The reddish regions surrounding the K, O, and H atoms represent intermolecular interactions with distances shorter than the  $r_{vdW}$ . Conversely, the white and blue-shaded regions correspond to equivalent and more distant sites relative to  $r_{vdW}$  [33]. The isomorphous nature of the four crystals results in highly similar Hirshfeld surfaces, indicating that the contacts involved between the fragments  $[\text{V}/\text{M}'(\text{H}_2\text{O})_6]$ ,  $[\text{SO}_4]$ , and  $[\text{KO}_8]$  arise from the following interactions:  $\text{H}\cdots\text{O}/\text{O}\cdots\text{H}$ ,  $\text{K}\cdots\text{O}/\text{O}\cdots\text{K}$ , and  $\text{K}\cdots\text{H}/\text{H}\cdots\text{K}$ .

Using Hirshfeld surfaces, 2D fingerprint mappings were taken to quantify the percentage of each contact within the crystal lattice. These plots, depicted in Figure 2i–l, represent cumulative histograms based on the  $d_i$  and  $d_e$  parameters in the x and y coordinates, respectively. The colored dots on the surface pattern indicate close (red dots) and distant (blue dots) contacts [34]. Notably, a similarity is observed across all total histograms. However, a detailed analysis of these contacts reveals seven non-covalent bonds in all crystals, although with varying percentages.

Figure 2m–p depict the percentages of each contact in the crystal lattice for the mixed salts. Although these salts are isostructural, the values of each intermolecular interaction differ due to the features involved in the different coordination spheres of the hexahydrate complexes. The most predominant contacts arise from the  $\text{H}\cdots\text{O}/\text{O}\cdots\text{H}$  and  $\text{K}\cdots\text{O}/\text{O}\cdots\text{K}$  interactions, accounting for  $\approx 66.4$ ,  $66.2$ ,  $66.1$ , and  $66.0\%$  in KVCoSOH, KVNiSOH, KVCuSOH, and KVZnSOH crystals, respectively. Notably, the  $\text{H}\cdots\text{O}/\text{O}\cdots\text{H}$  contact represents the most intense interaction in these structures. The sharp peaks concentrated in the  $d_i$  versus  $d_e$  low value range in Figure 2i–l characterize such behavior. Usually, in Tutton salts,  $\text{H}\cdots\text{O}/\text{O}\cdots\text{H}$  hydrogen bonds play a crucial role in thermo-structural stability, owing to the robust nature of these intermolecular forces, which is why they tend to present in greater quantities than

the others [35]. The percentages of non-covalent H $\cdots$ O/O $\cdots$ H and K $\cdots$ O/O $\cdots$ K bonds demonstrated here are consistent with those reported in the literature for similar structures, such as K<sub>2</sub>Mn<sub>0.03</sub>Ni<sub>0.97</sub>(SO<sub>4</sub>)<sub>2</sub>(H<sub>2</sub>O)<sub>6</sub> and K<sub>2</sub>Mn<sub>0.18</sub>Cu<sub>0.82</sub>(SO<sub>4</sub>)<sub>2</sub>(H<sub>2</sub>O)<sub>6</sub>, where a predominance of more than 60% of these intermolecular interactions involved in the crystal lattice was also observed [24].

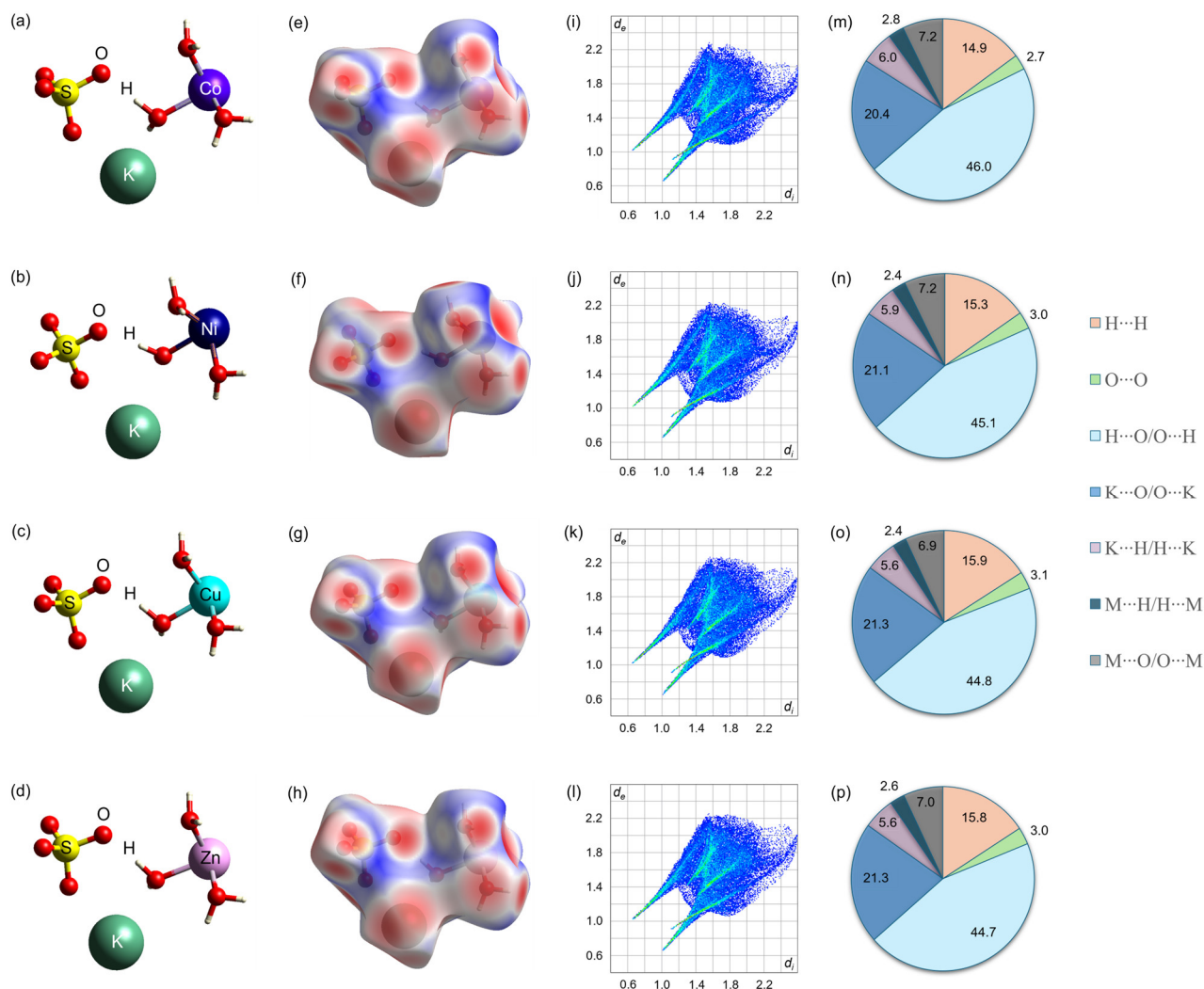


**Figure 2.** Asymmetric unit of (a) KVCuSOH, (b) KVNiSOH, (c) KVCuSOH, and (d) KVZnSOH. Hirshfeld surface mapping based on  $d_{norm}$ : (e) KVCuSOH, (f) KVNiSOH, (g) KVCuSOH, and (h) KVZnSOH. Cumulative 2D fingerprint plots: (i) KVCuSOH, (j) KVNiSOH, (k) KVCuSOH, and (l) KVZnSOH. Contribution percentage associated with specific contacts calculated from fingerprint plots: (m) KVCuSOH, (n) KVNiSOH, (o) KVCuSOH, and (p) KVZnSOH.

In addition to the interactions mentioned earlier, the Tutton salts exhibit intermediate non-covalent bonds involving the H $\cdots$ H (dispersive force), M' $\cdots$ O/O $\cdots$ M' (ionic bond), and K $\cdots$ H/H $\cdots$ K (dipole-ion) contacts. Such contacts contribute to the lattice structure with  $\approx$ 281% for KVCuSOH and 28.4% for KVNiSOH, KVCuSOH, and KVZnSOH crystals. Less significant contacts (O $\cdots$ O; M' $\cdots$ H/H $\cdots$ M') were recorded with percentages lower than 3.1%. It is important to highlight that the differences found here correlate with the geometric parameters of bond lengths and angles computed by PXRD.

### 3.3. Crystal Void Study

To further describe the unit cell of mixed salts, an additional computational study was conducted based on the analysis of crystal voids using electron density isosurfaces

with 0.02 a.u. (see Figure 3). Estimating the volume of total voids and their respective percentages, surface area, globularity, and asphericity indices was possible.

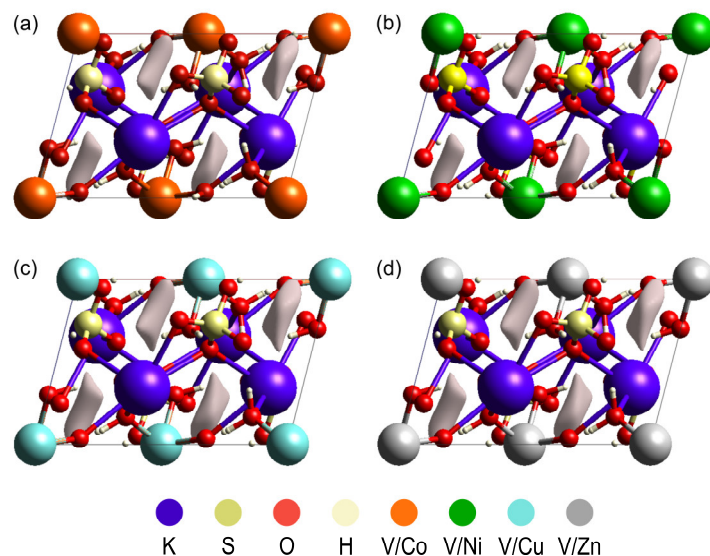


**Figure 3.** Calculated crystal voids (viewed along the *a-c* planes of the unit cells) for the mixed Tutton salts: (a) KVCoSOH, (b) KVNiSOH, (c) KVCuSOH, and (d) KVZnSOH.

Figure 3a–d show the mappings of minimum voids in unit cells. The isosurfaces are equivalent to areas ranging from 21.32 to 28.52 Å<sup>2</sup>. It should be noted that the projected isosurfaces are not entirely close between the free spaces because they are areas where intermolecular interactions occur between the molecular layers.

The KVCoSOH and KVNiSOH salts present the lowest percentages of free spaces of the order of less than 1%, being  $\approx 0.63\% \equiv 4.13 \text{ \AA}^3$  and  $0.53\% \equiv 3.41 \text{ \AA}^3$ , respectively. KVCuSOH ( $0.81\% \equiv 5.31 \text{ \AA}^3$ ) and KVZnSOH ( $0.76\% \equiv 4.98 \text{ \AA}^3$ ) show slightly higher values. Since the lowest percentages belong to the KVCoSOH and KVNiSOH salts, these exhibit a greater interlayer interaction energy and a higher thermo-structural stability when compared to the KVZnSOH and KVCuSOH salts. In general, the calculated values indicate that the chemical species of these mixed Tutton salts have high lattice energy and close specific contacts between the layers.

The slight differences observed are attributed to the physicochemical properties associated with the distinct coordination spheres, their corresponding mixed occupancy factors, and the electronegativity of the transition metals. Additionally, due to the low percentage of voids, only small impurities can be introduced into these crystals to modulate or tune properties of interest. Indeed, the void percentage in the unit cell is directly linked to the physical and chemical properties of a material, mainly the structural, vibrational, and thermal ones, as observed for the  $(\text{NH}_4)_2\text{Mn}_{0.5}\text{Zn}_{0.5}(\text{SO}_4)_2(\text{H}_2\text{O})_6$  crystal [17]. Table 5 lists the cell voids in volume, percentage, and areal terms in addition to the globularity and asphericity indices for the KVM'SOH salts. Both globularity and asphericity are related to the shape of particles. Globularity evaluates how closely particles resemble an ideal spherical shape, while asphericity describes how spherical a given object is. These descriptors range from 0 to 1, with values close to 0 indicating perfectly spherical and globular particles and values close to 1 characterizing elongated or non-spherical particles [33].

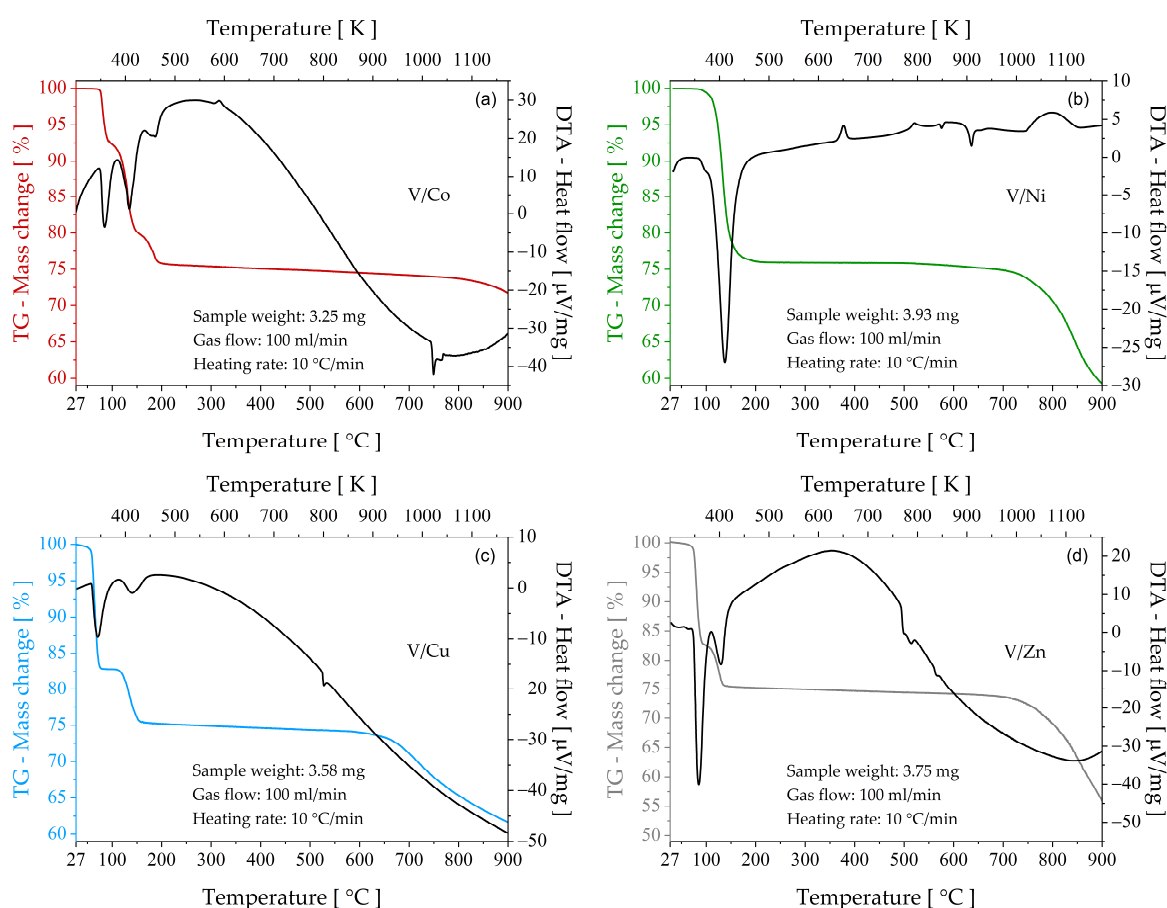


**Table 5.** Cell voids, globularity, and asphericity computed for the mixed KVM'SOH Tuttons.

Sample	Unit Cell [Å <sup>3</sup> ]	Voids [Å <sup>3</sup> ]	Voids [%]	Voids Surface Area [Å <sup>2</sup> ]	Globularity	Asphericity
KVCoSOH	653.12	4.13	0.63	24.17	0.51	0.46
KVNiSOH	645.26	3.41	0.53	21.32	0.46	0.47
KVCuSOH	659.42	5.31	0.81	28.52	0.51	0.43
KVZnSOH	655.59	4.98	0.76	27.42	0.47	0.44

### 3.4. Thermal Characterization

The thermo-structural behavior was evaluated using a TG-DTA (Shimadzu, Tokyo, Japan). Figure 4 shows the coupled thermograms in a temperature range between 27 and 900 °C. The TG curves indicate that the KVCoSOH (74 °C) and KVNiSOH (85 °C) crystals are the most thermally stable. On the other hand, KVCuSOH and KVZnSOH show a mass loss above 55–57 °C. In addition to being related to the effect of random occupation of transition metals in the divalent sites, the differences in stability are also associated with intermolecular interactions via hydrogen bonds, as discussed in Section 3.2.

**Figure 4.** Coupled TG-DTA thermograms of the mixed Tutton salts: (a) KVCoSOH, (b) KVNiSOH, (c) KVCuSOH, and (d) KVZnSOH.

As the temperature increased, all mixed salts underwent a dehydration process by releasing six H<sub>2</sub>O molecules. However, this process occurred at different stages for each sample. KVCoSOH degradation occurred in three steps between 74 and 220 °C. The first mass loss corresponded to the release of two H<sub>2</sub>O molecules, the second to three H<sub>2</sub>O molecules, and the third to one H<sub>2</sub>O molecule. The endothermic peaks at 85, 134, and 187 °C confirm the dehydration process of the hexahydrate phase in several steps. In

contrast, KVNiSOH exhibited complete dehydration between 85 and 200 °C in a single stage. The intense endothermic peak around 138 °C (DTA curve) also identified the event.

The KVCuSOH and KNZnSOH crystals showed similar thermal behavior. In the 55–107 °C interval, both released four H<sub>2</sub>O molecules and, between 107 and 220 °C, lost the remaining two H<sub>2</sub>O molecules. Two endothermic DTA peaks accompanied such events. Table 6 summarizes the thermal events observed for the mixed KVM'SOH Tutton salts.

**Table 6.** Thermal events observed in TG-DTA curves for mixed KVM'SOH Tutton salts.

Sample	TG			DTA		
	$\Delta T$ [°C]	Weight Loss [%]	Weight Loss [g/mol]	Molecular Fragment	T <sub>peak</sub> [°C]	Thermal Event
KVCuSOH	74–220	24.37	105.6	≈6 H <sub>2</sub> O	85 134 187 316	dehydration dehydration dehydration crystallization
	220–900	23.65	102.5	≈SO <sub>3</sub> + O	749 765	transition V/CoSO <sub>4</sub> melting
KVNiSOH	85–200	24.01	104.3	≈6 H <sub>2</sub> O	138 378 520	dehydration crystallization --
	200–900	19.98	73.6	≈SO <sub>3</sub>	575 635 798	transition V/NiSO <sub>4</sub> melting decomposition
KVCuSOH	57–220	24.55	107.1	≈6 H <sub>2</sub> O	71 141	dehydration dehydration
	220–900	16.88	73.6	≈SO <sub>3</sub>	528	transition
KVZnSOH	55–220	25.01	109.18	≈6 H <sub>2</sub> O	85 130 499	dehydration dehydration --
	220–900	19.92	86.99	≈SO <sub>3</sub>	515 565	transition V/ZnSO <sub>4</sub> melting

After structural transformation from the hexahydrate phase to the anhydrous form, the dehydrate salts remained thermally stable (without apparent mass loss) up to ≈700–800 °C. However, endothermic and exothermic DTA events characteristic of phase transitions via crystallization, symmetry change, or melting were observed, as very well described in the literature for potassium-based Tutton salts [36–39]. At temperatures higher than 700–800 °C, decomposition of the metal sulfates occurs.

### 3.5. Thermochemical Parameters via DSC Analysis

Additional thermoanalytical experiments were conducted via DSC to complement the TG-DTA studies. The dehydration performance was evaluated by targeting thermochemical heat storage applications. For this, the dehydration reaction enthalpy ( $\Delta H$ ) was estimated using the TA-60WS software, as shown in the highlighted region in Figure 5a–d. The DSC curves show the same endothermic events observed in the DTA curves in the 27–215 °C range.

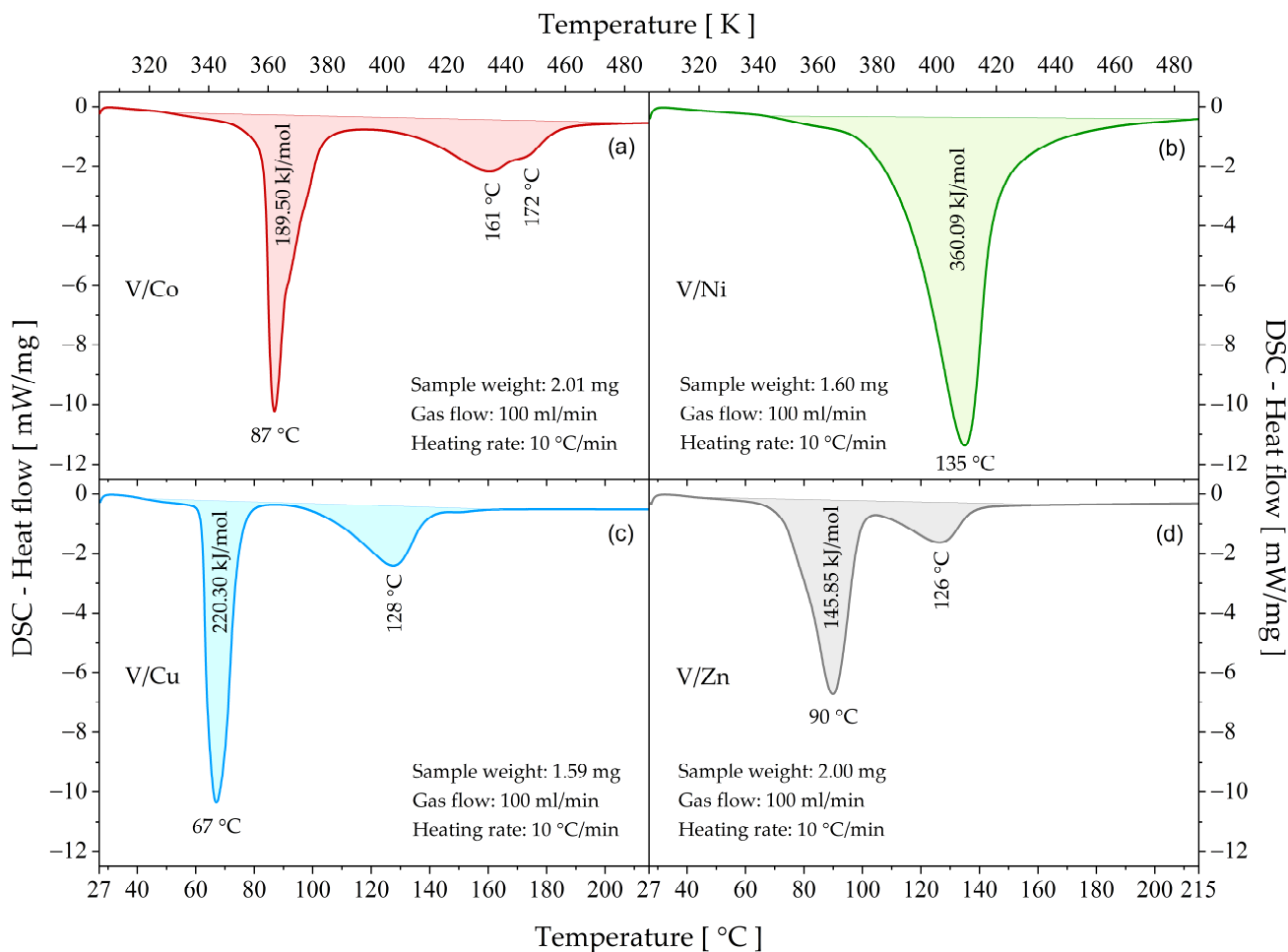


**Figure 5.** DSC analyses of mixed Tutton salts: (a) KVCoSOH, (b) KVNiSOH, (c) KVCuSOH, and (d) KVZnSOH.

Despite the crystals being isostructural, the heat involved in the dehydration process varied greatly between samples, as shown in Table 7. The data indicate that the KVCoSOH (189.50 kJ/mol), KVCuSOH (220.30 kJ/mol), and KVZnSOH (145.85 kJ/mol) salts exhibit low dehydration enthalpies. In other words, even though the six H<sub>2</sub>O molecules are coordinated to the V/Co, V/Cu, and V/Zn metal complexes, low energies in the heat form can break the metal–ligand bonds. In contrast, further energy is needed to release H<sub>2</sub>O from the KVNiSOH crystal (360.09 kJ/mol).

**Table 7.** Evaluated parameters (via DSC) considered for thermochemical applications.

Sample	T <sub>peak</sub> [°C]	ΔH <sub>exp</sub> [kJ/mol]	ΔH <sub>exp</sub> [kJ/H <sub>2</sub> O mol]	MM <sub>Salt</sub> [g/mol]	ρ <sub>Salt</sub> [g/cm <sup>3</sup> ]	ΔH <sub>V</sub> [GJ/m <sup>3</sup> ]
KVCoSOH	87, 161, and 172	189.50	31.58	433.495	2.224	0.972
KVNiSOH	135	360.09	60.02	433.448	2.210	1.836
KVCuSOH	67 and 128	220.30	36.72	436.398	2.163	1.091
KVZnSOH	90 and 126	145.85	24.31	436.703	2.248	0.751

The volumetric energy storage density—ΔH<sub>V</sub> (amount of energy stored per unit volume in J/m<sup>3</sup>)—was calculated based on the research conducted by N'Tsoukpo and

Ousaleh [40,41]. The data required to obtain this parameter were taken from the DSC and PXRD results.  $\Delta H_V$  was valued as follows:

$$\Delta H_V = \frac{\Delta H_{\text{exp}}}{MM_{\text{Salt}}} \rho_{\text{Salt}}$$

where  $\Delta H_{\text{exp}}$  (in J/mol) corresponds to the experimental dehydration enthalpy.  $MM_{\text{Salt}}$  (g/mol) and  $\rho_{\text{Salt}}$  (g/cm<sup>3</sup>) are the molar mass and volumetric mass density of the mixed Tutton salts, respectively. The calculated  $\Delta H_V$  values are given in Table 7.

According to previously established criteria in the literature [14], potential materials for thermochemical energy storage devices must present a dehydration temperature of  $\leq 120$  °C and an energy density of  $\geq 1.3$  GJ/m<sup>3</sup>. In this scenario, only the KVNiSOH crystal meets both criteria, with a thermal stability of  $\approx 85$  °C and an energy storage density of  $\approx 1.84$  GJ/m<sup>3</sup>. When compared with the individual Tutton salt  $K_2Ni(SO_4)_2(H_2O)_6$  (1.78 GJ/m<sup>3</sup>) [14], the value was slightly improved ( $\approx 0.06$  GJ/m<sup>3</sup>), supposedly due to the mixing effect of the V<sup>2+</sup> and Ni<sup>2+</sup> ions introduced at the bivalent sites—an effect not observed for the other mixed crystals based on Co, Cu, and Zn.

In short, comparing the four mixed KVM'SOH salts, V/Ni exhibited suitable dehydration behavior, and the high energy storage density required for thermochemical applications at a domestic level. However, further investigations must be performed to verify the reversibility of the dehydration/hydration reaction and cycling stability.

#### 4. Conclusions

In this paper, four novel mixed Tutton salts with compositions of  $K_2V_{0.48}Co_{0.52}(SO_4)_2(H_2O)_6 \equiv KVCuSOH$ ,  $K_2V_{0.47}Ni_{0.53}(SO_4)_2(H_2O)_6 \equiv KVNiSOH$ ,  $K_2V_{0.44}Cu_{0.56}(SO_4)_2(H_2O)_6 \equiv KVCuSOH$ , and  $K_2V_{0.49}Zn_{0.51}(SO_4)_2(H_2O)_6 \equiv KVZnSOH$  were successfully grown by the isothermal evaporation technique. The crystallographic structures were solved by PXRD and Rietveld refinement, where it was also possible to determine the occupancy factors between the divalent cations (V<sup>2+</sup>, Co<sup>2+</sup>, Ni<sup>2+</sup>, Cu<sup>2+</sup>, and Zn<sup>2+</sup>) on the crystal lattice. Differences in the physicochemical properties of the divalent ions favor geometric distortions around the coordination spheres, originating from the Jahn–Teller effect. All mixed salts crystallize in monoclinic symmetry ( $P2_1/a$ ) with two  $(K_2V_{1-x}M'_x(SO_4)_2(H_2O)_6)$  formulas per unit cell. The crystal structures were deposited in the CCDC database under the codes 2363950 (KVCuSOH), 2363949 (KVNiSOH), 2363947 (KVCuSOH), and 2363946 (KVZnSOH). Structural information can be found in Supplementary Materials S1–S4.

Computational investigations using Hirshfeld surfaces and 2D fingerprint plots were performed to elucidate and quantify the intermolecular interactions between the molecular layers. It was found that the main contacts that stabilize the crystal lattice of the vanadium-based Tutton salts are the hydrogen bond (H $\cdots$ O/O $\cdots$ H) and ion–dipole (K $\cdots$ O/O $\cdots$ K) types. Additionally, the free spaces of the primitive unit cells were estimated by electron density isosurfaces in which a low percentage of voids was determined for all structures, indicating high lattice energies between the constituent chemical species.

The thermoanalytical experiments showed that the V/Co, V/Ni, V/Cu, and V/Zn crystals have thermal stability up to around 74, 85, 57, and 55 °C, respectively. Above these temperatures, the salts exhibited several physicochemical changes associated with transformation and phase transition processes, such as dehydration and crystallization. The dehydration reaction enthalpies and energy storage densities were estimated from the DSC thermograms. The findings indicate that only the KVNiSOH crystal meets the criteria of an energy storage density of  $\geq 1.3$  GJ/m<sup>3</sup> and a dehydration temperature of  $\leq 120$  °C. KVNiSOH showed a thermal stability of  $\approx 85$  °C and an energy storage density of  $\approx 1.84$  GJ/m<sup>3</sup>.

**Supplementary Materials:** The information associated with the four solved structures deposited in the CCDC database can be downloaded at <https://www.mdpi.com/article/10.3390/physchem4030022/s1> through Supplementary Materials S1–S4—Crystallographic parameters obtained for the salts

KVCoSOH (S1), KVNiSOH (S2), KVCuSOH (S3), and KVZnSOH (S4) from the structures solved via PXRD and Rietveld refinement.

**Author Contributions:** Conceptualization, J.G.d.O.N. and A.O.d.S.; methodology, J.G.d.O.N. and J.V.M.; software, J.G.d.O.N. and J.V.M.; validation, J.G.d.O.N., R.L. and A.O.d.S.; formal analysis, R.L. and A.O.d.S.; investigation, J.G.d.O.N., J.V.M., J.C.d.S., R.L. and A.O.d.S.; resources, R.L. and A.O.d.S.; data curation, J.G.d.O.N., J.V.M., J.C.d.S., R.L. and A.O.d.S.; writing—original draft preparation, J.G.d.O.N. and J.V.M.; writing—review and editing, J.G.d.O.N., R.L. and A.O.d.S.; visualization, J.G.d.O.N., J.V.M., J.C.d.S., R.L. and A.O.d.S.; supervision, R.L. and A.O.d.S.; project administration, R.L. and A.O.d.S.; funding acquisition, R.L. and A.O.d.S. All authors have read and agreed to the published version of the manuscript.

**Funding:** This research was funded by Fundação de Amparo à Pesquisa e ao Desenvolvimento Científico e Tecnológico do Maranhão (FAPEMA), grant number BPD-12643/22; Coordenação de Aperfeiçoamento de Pessoal de Nível Superior (CAPES), grant number 001; and the National Council for Scientific and Technological Development (CNPq), grant numbers 312926/2020-0 and 317469/2021-5.

**Data Availability Statement:** Crystal structure information is available at [www.ccdc.cam.ac.uk](http://www.ccdc.cam.ac.uk) (accessed on 20 July 2024) and in the Cambridge Structural Database under the numbers 2363950 (KVCoSOH), 2363949 (KVNiSOH), 2363947 (KVCuSOH), and 2363946 (KVZnSOH).

**Acknowledgments:** The authors thank the following Brazilian agencies for providing financial support: FAPEMA, CAPES, and CNPq.

**Conflicts of Interest:** The authors declare that they have no known competing financial interests or personal relationships that could have appeared to influence the work reported in this paper.

## References

1. Liu, W.; Song, M.S.; Kong, B.; Cui, Y. Flexible and Stretchable Energy Storage: Recent Advances and Future Perspectives. *Adv. Mater.* **2017**, *29*, 1603436. [[CrossRef](#)]
2. Zhang, W.; Xu, J. Advanced Lightweight Materials for Automobiles: A Review. *Mater. Des.* **2022**, *221*, 110994. [[CrossRef](#)]
3. Gao, M.; Gao, Y.; Chen, G.; Huang, X.; Xu, X.; Lv, J.; Wang, J.; Xu, D.; Liu, G. Recent Advances and Future Trends in the Detection of Contaminants by Molecularly Imprinted Polymers in Food Samples. *Front. Chem.* **2020**, *8*, 616326. [[CrossRef](#)] [[PubMed](#)]
4. Wang, X.; Lu, X.; Liu, B.; Chen, D.; Tong, Y.; Shen, G. Flexible Energy-Storage Devices: Design Consideration and Recent Progress. *Adv. Mater.* **2014**, *26*, 4763–4782. [[CrossRef](#)] [[PubMed](#)]
5. Choi, C.; Kim, S.; Kim, R.; Choi, Y.; Kim, S.; Jung, H.-Y.; Yang, J.H.; Kim, H.-T. A Review of Vanadium Electrolytes for Vanadium Redox Flow Batteries. *Renew. Sustain. Energy Rev.* **2017**, *69*, 263–274. [[CrossRef](#)]
6. Badmaev, V.; Prakash, S.; Majeed, M. Vanadium: A Review of Its Potential Role in the Fight against Diabetes. *J. Altern. Complement. Med.* **1999**, *5*, 273–291. [[CrossRef](#)] [[PubMed](#)]
7. Floris, B.; Sabuzi, F.; Coletti, A.; Conte, V. Sustainable Vanadium-Catalyzed Oxidation of Organic Substrates with H<sub>2</sub>O<sub>2</sub>. *Catal. Today* **2017**, *285*, 49–56. [[CrossRef](#)]
8. Zou, Z.; Li, N.; Li, D.; Liu, H.; Mu, S. A Vanadium-Based Conversion Coating as Chromate Replacement for Electroplated Steel Substrates. *J. Alloys Compd.* **2011**, *509*, 503–507. [[CrossRef](#)]
9. Galloni, P.; Conte, V.; Floris, B. A Journey into the Electrochemistry of Vanadium Compounds. *Coord. Chem. Rev.* **2015**, *301–302*, 240–299. [[CrossRef](#)]
10. Larkworthy, L.F.; Murphy, J.M.; Patel, K.C.; Phillips, D.J. Vanadium(II) Chemistry. Part I. Magnetic and Spectroscopic Investigations of the Sulphate and Double Sulphates. *J. Chem. Soc. A.* **1968**, *12*, 2936–2938. [[CrossRef](#)]
11. Montgomery, H.; Morosin, B.; Natt, J.J.; Witkowska, A.M.; Lingafelter, E.C. The Crystal Structure of Tutton's Salts. VI. Vanadium(II), Iron(II) and Cobalt(II) Ammonium Sulfate Hexahydrates. *Acta Crystallogr.* **1967**, *22*, 775–780. [[CrossRef](#)]
12. Oliveira Neto, J.G.; Lang, R.; Rodrigues, J.A.O.; Gutiérrez, C.E.O.; Murillo, M.A.R.; Sousa, F.F.; Silva Filho, J.G.; Santos, A.O. Kröhnkite-Type K<sub>2</sub>Mn(SO<sub>4</sub>)<sub>2</sub>(H<sub>2</sub>O)<sub>2</sub> Double Salt: Synthesis, Structure, and Properties. *J. Mater. Sci.* **2022**, *57*, 8195–8210. [[CrossRef](#)]
13. Donkers, P.A.J.; Sögütoglu, L.C.; Huinink, H.P.; Fischer, H.R.; Adan, O.C.G. A Review of Salt Hydrates for Seasonal Heat Storage in Domestic Applications. *Appl. Energy* **2017**, *199*, 45–68. [[CrossRef](#)]
14. Kooijman, W.; Kok, D.J.; Blijlevens, M.A.R.; Meekes, H.; Vlieg, E. Screening Double Salt Sulfate Hydrates for Application in Thermochemical Heat Storage. *J. Energy Storage* **2022**, *55*, 105459. [[CrossRef](#)]
15. Souamti, A.; Zayani, L.; Lozano-Gorrin, A.D.; Ben Hassen Chehimi, D.; Morales Palomino, J. Synthesis, Characterization and Thermal Behavior of New Rare Earth Ion-Doped Picromerite-Type Tutton's Salts. *J. Therm. Anal. Calorim.* **2017**, *128*, 1001–1008. [[CrossRef](#)]

16. Ghosh, S.; Ullah, S.; de Mendonça, J.P.A.; Moura, L.G.; Menezes, M.G.; Flôres, L.S.; Pacheco, T.S.; de Oliveira, L.F.C.; Sato, F.; Ferreira, S.O. Electronic Properties and Vibrational Spectra of  $(\text{NH}_4)_2\text{M}''(\text{SO}_4)_2 \cdot 6\text{H}_2\text{O}$  ( $\text{M} = \text{Ni}, \text{Cu}$ ) Tutton's Salt: DFT and Experimental Study. *Spectrochim. Acta-Part A Mol. Biomol. Spectrosc.* **2019**, *218*, 281–292. [[CrossRef](#)]
17. Neto, J.G.O.; Viana, J.R.; Lopes, J.B.O.; Lima, A.D.S.G.; Sousa, M.L.; Lage, M.R.; Stoyanov, S.R.; Lang, R.; Santos, A.O. Crystal Growth, Crystal Structure Determination, and Computational Studies of a New Mixed  $(\text{NH}_4)_2\text{Mn}_{1-x}\text{Zn}_x(\text{SO}_4)_2(\text{H}_2\text{O})_6$  Tutton Salt. *J. Mol. Model.* **2022**, *28*, 341. [[CrossRef](#)]
18. De Oliveira, G.; Carvalho, J.D.O.; Marques, J.V.; Façanha, P.F.; Adenilson, O.; Lang, R. Tutton  $\text{K}_2\text{Zn}(\text{SO}_4)_2(\text{H}_2\text{O})_6$  Salt: Structural-Vibrational Properties as a Function of Temperature and Ab Initio Calculations. *Spectrochim. Acta-Part A Mol. Spectrosc.* **2024**, *306*, 123611. [[CrossRef](#)]
19. Dobe, C.; Strässle, T.; Juranyi, F.; Tregenna-Piggott, P.L.W. Pressure-Induced Switch of the Direction of the Unique Jahn-Teller Axis of the Chromium(II) Hexaqua Cation in the Deuterated Ammonium Chromium Tutton Salt. *Inorg. Chem.* **2006**, *45*, 5066–5072. [[CrossRef](#)]
20. Augustyniak, M.A.; Usachev, A.E. The Host Lattice Influence on the Jahn-Teller Effect of the  $\text{Cu}(\text{H}_2\text{O})_6^{2+}$  Complex Studied by EPR in  $\text{K}_2\text{Zn}(\text{SO}_4)_2 \cdot 6\text{H}_2\text{O}$  and  $(\text{NH}_4)_2\text{Zn}(\text{SO}_4)_2 \cdot 6\text{H}_2\text{O}$  Tutton Salt Crystals. *J. Phys. Condens. Matter* **1999**, *11*, 4391–4400. [[CrossRef](#)]
21. Pacheco, T.S.; Ludwig, Z.M.C.; Sant'Anna, D.R.; Perpétuo, G.J.; Franco, C.J.; Paiva, E.C.; Ghosh, S. Growth and Vibrational Spectroscopy of  $\text{K}_2\text{Li}_y\text{Ni}_x\text{Co}_{1-x}\text{SO}_4 \cdot 6\text{H}_2\text{O}$  ( $Y = 0.1; 0.2; 0.3; 0.4$ ) Crystals. *Vib. Spectrosc.* **2020**, *109*, 103093. [[CrossRef](#)]
22. No, R.; St, J.; Rani, C.S.; Sweetlin, M.D.; Selvarajan, P. Studies of L-Methionine Doped Ammonium Ferrous Sulfate Single Crystals Grown by Solution Method. *IJRAR—Int. J. Res. Anal. Rev.* **2018**, *5*, 615–622.
23. Ghosh, S.; Lima, A.H.; Flôres, L.S.; Pacheco, T.S.; Barbosa, A.A.; Ullah, S.; de Mendonça, J.P.A.; Oliveira, L.F.C.; Quirino, W.G. Growth and Characterization of Ammonium Nickel-Copper Sulfate Hexahydrate: A New Crystal of Tutton's Salt Family for the Application in Solar-Blind Technology. *Opt. Mater.* **2018**, *85*, 425–437. [[CrossRef](#)]
24. De Oliveira, G.; Viana, J.R.; Lima, A.D.S.G.; Lopes, J.B.O.; Ayala, A.P.; Lage, M.R.; Stoyanov, S.R.; Santos, A.O. Assessing the Novel Mixed Tutton Salts for Thermochemical Heat Storage Applications: An Experimental—Theoretical Study. *Molecules* **2023**, *97*, 8058. [[CrossRef](#)]
25. Smith, J.; Weinberger, P.; Werner, A. Dehydration Performance of a Novel Solid Solution Library of Mixed Tutton Salts as Thermochemical Heat Storage Materials. *J. Energy Storage* **2024**, *78*, 110003. [[CrossRef](#)]
26. David, W.I.F.; Shankland, K.; Van De Streek, J.; Pidcock, E.; Motherwell, W.D.S.; Cole, J.C. DASH: A Program for Crystal Structure Determination from Powder Diffraction Data. *J. Appl. Crystallogr.* **2006**, *39*, 910–915. [[CrossRef](#)]
27. Le Bail, A.; Duroy, H.; Fourquet, J.L. Ab-initio structure determination of  $\text{LiSbWO}_6$  by X-ray powder diffraction. *Mat. Res. Bull.* **1988**, *23*, 447–452. [[CrossRef](#)]
28. Mccusker, L.B.; Von Dreele, R.B.; Cox, D.E.; Louër, D.; Scardi, P. Rietveld Refinement Guidelines. *J. Appl. Crystallogr.* **1999**, *32*, 36–50. [[CrossRef](#)]
29. Allen, F.H.; Johnson, O.; Shields, G.P.; Smith, B.R.; Towler, M. CIF Applications. XV. EnCIFer: A Program for Viewing, Editing and Visualizing CIFs. *J. Appl. Crystallogr.* **2004**, *37*, 335–338. [[CrossRef](#)]
30. Turner, M.J.; McKinnon, J.J.; Wolff, S.K.; Gromwood, D.J.; Spackman, P.R.; Jayalitaka, D.; Spackman, M.A. *Crystal Explorer 17.5*; University of Western Australia: Perth, WA, Australia, 2017.
31. Seth, S.K.; Sarkar, D.; Roy, A.; Kar, T. Insight into Supramolecular Self-Assembly Directed by Weak Interactions in Acetophenone Derivatives: Crystal Structures and Hirshfeld Surface Analyses. *CrystEngComm* **2011**, *13*, 6728–6741. [[CrossRef](#)]
32. Turner, M.J.; McKinnon, J.J.; Jayatilaka, D.; Spackman, M.A. Visualisation and Characterisation of Voids in Crystalline Materials. *CrystEngComm* **2011**, *13*, 1804–1813. [[CrossRef](#)]
33. de Oliveira Neto, J.G.; Viana, J.R.; Ayala, A.P.; Nogueira, C.E.S.; de Oliveira, M.M.; dos Santos, A.O.; de Sousa, F.F. Crystallographic, Intermolecular Interactions, Vibrational, and Computational Studies of a New Cocrystal of Decanoic Acid and Nicotinamide. *J. Mol. Struct.* **2024**, *1315*, 138835. [[CrossRef](#)]
34. Cardoso, L.M.B.; de Oliveira Neto, J.G.; Saraiva, G.D.; Leite, F.F.; Ayala, A.P.; dos Santos, A.O.; de Sousa, F.F. New Polymorphic Phase of Arachidic Acid Crystal: Structure, Intermolecular Interactions, Low-Temperature Stability and Raman Spectroscopy Combined with DFT Calculations. *RSC Adv.* **2023**, *13*, 34032–34044. [[CrossRef](#)] [[PubMed](#)]
35. Gomes, J.; Neto, D.O.; Fernando, L.; Kalil, T.; Alves, C.; Neumann, A.; De Sousa, F.F.; Ayala, A.P. Mixed Tutton Salts  $\text{K}_2\text{Mn}_{0.15}\text{Co}_{0.85}(\text{SO}_4)_2(\text{H}_2\text{O})_6$  and  $\text{K}_2\text{Mn}_{0.16}\text{Zn}_{0.84}(\text{SO}_4)_2(\text{H}_2\text{O})_6$  for Applications in Thermochemical Devices: Experimental Physicochemical Properties Combined with First-principles Calculations. *J. Mater. Sci.* **2024**, *59*, 14445–14464. [[CrossRef](#)]
36. Souamti, A.; Martín, I.R.; Zayani, L.; Hernández-Rodríguez, M.A.; Soler-Carracedo, K.; Lozano-Gorrín, A.D.; Lalla, E.; Chehimi, D.B.H. Synthesis, Characterization and Spectroscopic Properties of a New  $\text{Nd}^{3+}$ -Doped Co-Picromerite-Type Tutton Salt. *J. Lumin.* **2016**, *177*, 93–98. [[CrossRef](#)]
37. Souamti, A.; Martín, I.R.; Zayani, L.; Lozano-Gorrín, A.D.; Ben Hassen Chehimi, D. Luminescence Properties of  $\text{Pr}^{3+}$  Ion Doped Mg-Picromerite Tutton Salt. *J. Lumin.* **2017**, *188*, 148–153. [[CrossRef](#)]
38. Lim, A.R. Thermodynamic Properties and Phase Transitions of Tutton Salt  $(\text{NH}_4)_2\text{Co}(\text{SO}_4)_2 \cdot 6\text{H}_2\text{O}$  Crystals. *J. Therm. Anal. Calorim.* **2012**, *109*, 1619–1623. [[CrossRef](#)]
39. Morales, A.C.; Cooper, N.D.; Reisner, B.A.; DeVore, T.C. Variable Temperature PXRD Investigation of the Phase Changes during the Dehydration of Potassium Tutton Salts. *J. Therm. Anal. Calorim.* **2018**, *132*, 1523–1534. [[CrossRef](#)]

40. N'Tsoukpoe, K.E.; Schmidt, T.; Rammelberg, H.U.; Watts, B.A.; Ruck, W.K.L. A Systematic Multi-Step Screening of Numerous Salt Hydrates for Low Temperature Thermochemical Energy Storage. *Appl. Energy* **2014**, *124*, 1–16. [[CrossRef](#)]
41. Ait Ousaleh, H.; Sair, S.; Zaki, A.; Faik, A.; Mirena Igartua, J.; El Bouari, A. Double Hydrates Salt as Sustainable Thermochemical Energy Storage Materials: Evaluation of Dehydration Behavior and Structural Phase Transition Reversibility. *Sol. Energy* **2020**, *201*, 846–856. [[CrossRef](#)]

**Disclaimer/Publisher's Note:** The statements, opinions and data contained in all publications are solely those of the individual author(s) and contributor(s) and not of MDPI and/or the editor(s). MDPI and/or the editor(s) disclaim responsibility for any injury to people or property resulting from any ideas, methods, instructions or products referred to in the content.